Journal of Nuclear Materials 396 (2010) 86–93

Contents lists available at ScienceDirect

Journal of Nuclear Materials

journal homepage: www.elsevier.com/locate/jnucmat

Formation of oxides particles in ferritic steel by using gas-atomized powder

Yong Liu [a,*], Jinghua Fang [a], Donghua Liu [a], Zhi Lu [a], Feng Liu [a], Shiqi Chen [a], C.T. Liu [b]

[a] State Key Laboratory of Powder Metallurgy, Central South University, Changsha 410083, PR China
[b] Department of Mechanical Engineering, Hongkong Polytechnic University, Hong Kong, PR China

ARTICLE INFO

Article history:
Received 30 April 2009
Accepted 23 October 2009

Keywords:
Oxides dispersion strengthening
Ferritic steel
Recrystallization
Hardness

ABSTRACT

Oxides dispersion strengthened (ODS) ferritic steel was prepared by using gas-atomized pre-alloyed powder, without the conventional mechanical alloying process. By adjusting the volume content of O_2 in the gas atmosphere Ar, the O level in the ferritic powder can be well controlled. The O dissolves uniformly in the ferritic powder, and a very thin layer of oxides forms on the powder surface. After hot deformation, the primary particle boundaries, which retain after sintering, can be disintegrated and near fully dense materials can be obtained. The oxide layer on the powder surface has a significant effect on the microstructural evolution. It may prevent the diffusion in between the primary particles during sintering, and may dissolve and/or induce the nucleation of new oxides in the ferritic matrix during recrystallization. Two kinds of oxide particles are found in the ferritic steel: large (~100 nm) Ti-rich and fine (10–20 nm) Y–Ti-rich oxides. The hardness of the ferritic steel increases with increasing annealing temperatures, however, decreases at 1400 °C, due to the coarsening of precipitates and the recrystallization microstructure.

1. Introduction

Oxide dispersion strengthened (ODS) ferritic steels are very attractive materials for high temperature applications in nuclear reactors and gas turbines [1–4]. The fine or super-fine secondary particles dispersed in the matrix alloy usually have the following beneficial effects [5]: (1) pinning dislocations inside grains by Orowan mechanism; (2) stabilizing grain boundaries and hindering grain growth, thus increasing the creep resistance; (3) trapping He and other radioactive particles in fine-scale bubbles to avoid swelling in nuclear applications. Since 1980s, many ODS ferritic steels have been developed. The earliest generation of commercial ODS steels are MA956 and MA957 developed by International Nickel Company [3,6]. Both of these two ODS steels have been successfully used in US nuclear reactors. By addition of Ti, Ukai et al. refined the size of oxide precipitates, and the alloy developed as 9Cr NTS has been successfully applied for fast-reactor-fuel cladding [7,8]. Recently, scientists in ORNL found that the precipitates in ODS ferritic steel can be as fine as 1–2 nm, and they are stable at 800 °C as long as 14,500 h [9]. The ODS ferritic steels, developed as 12YWT and 14YWT can decrease the creep rate at temperatures ranging from 650 to 900 °C by six orders of magnitude, as compared with conventional steels [10–13]. The ultra-high stability of these nanoclusters has drawn a high attention in the material field.

ODS ferritic steels are usually prepared via mechanical alloying of rapid solidified pre-alloyed powder and fine ceramic particles (Y_2O_3 and TiO_2), followed by such densification methods as hot extrusion, rolling or hot isostatic pressing [7,11,14]. The ceramic particles will decompose or dissolve in the alloy matrix during mechanical alloying, and will precipitate as fine or nanostructured particles at subsequent annealing steps [15]. Therefore, in preparation of ODS ferritic steels, mechanical alloy is a very important step by introducing precipitate-formation atoms in the alloy matrix. Considering this fact, if the precipitate-formation atoms, for example, Y, Ti and O are already in the alloy matrix, it could avoid the mechanical alloying step, which is known to be an expensive and time-consuming processing method. Furthermore, microstructure and chemical homogeneity is also a major concern for ODS materials. In view of the difficulties of ODS, we are seeking for an innovative way to process materials with fine dispersion of oxide particles.

In this paper, our approach is to dissolve oxygen and other solute atoms in alloy by powder metallurgy in controlled oxidising environments. Y, Ti and O can be added to the alloy during melting as they have enough solubility in liquid Fe. In addition, the precipitation of coarse oxide particles can be prevented or retarded via rapid solidification process, such as gas-atomization. During subsequent thermal processes, including sintering, hot working and annealing, fine oxide particles possibly precipitate out from the

* Corresponding author. Tel.: +86 731 8830406; fax: +86 731 8710855.
E-mail address: yonliu11@yahoo.com.cn (Y. Liu).

0022-3115/$ - see front matter © 2009 Elsevier B.V. All rights reserved.
doi:10.1016/j.jnucmat.2009.10.057

matrix. Based on these considerations, a modified process for preparing ODS ferritic steels was introduced and the effects of processing parameters on the formation of fine precipitates were studied.

2. Experimental

The nominal composition of the ferritic alloy is 14YWT: Fe–14Cr–3W–0.4Ti–0.25Y, wt.%. High-purity (>99%) Fe, Cr and W were used as raw materials, while Ti and Y were added in the form of alloyed Fe–Ti and Fe–Y. All the raw materials were induction melted to a master alloy with the composition of 14YWT, except the additional O content was adjusted in the subsequent gas-atomization process by controlling the volume percent of O_2 in high purity argon (99.99%). The master alloy was remelted at 1500 °C, and then the melt was atomized in O_2-added Ar at a pressure of 3 MPa. The pre-alloyed powder was compacted at room temperature at a pressure of 600 MPa, and then sintered in a vacuum of 1×10^{-3} Pa, at 1250 °C for 2 h. In order to eliminate residual porosity and primary particle boundaries, the sintered compact was hot-forged and then hot-rolled both at 900 °C. The as-deformed specimens were heat-treated at temperatures ranging from 900 to 1400 °C for 1 h for microstructural control.

The O content in the powder was analyzed by using a TCH-600 H/N/O determinator. The surface morphology of powder was directly observed with a JSM-6360 LV Scanning Electron Microscope. In order to study the microstructure, some powder was mixed with resin and then polished. The O profile in the particles can be quantitatively determined by using Energy Diffraction X-ray Analyses (EDAX). The phase structures of the powder were determined by using a Rigaku D/max 2550VB$^+$ X-ray diffractometer, with a Cu–K, scanning at a voltage of 40 kV and a speed of 8°/min. The bulk specimens were sectioned and polished. The microstructure was also examined by SEM. The hardness of specimens was tested by using a A−200 Rockwell Hardness tester at a load of 1500 N, and the microhardness of specimens was tested by using a HVs-100 Vickers hardness tester at a load of 2 N. For more detailed study on the microstructures, a JEM-2100F Transmission Electron Microscopy was used, operating at 200 kV. Disk specimens were spark eroded from the bulk, polished on emery paper and then electro-polished by twin-jet with a solution containing 6%$HClO_4$ + 14%H_2O + 80%C_2H_5OH, vol.%. In order to determine the existence of nanoclusters, needle-like specimens were cut by using a Focused Ion Beam (FIB) instrument and then observed in a Groupe de Physique des Matériaux (UMR CNRS 6634-ERT1000)'s Atom Probe Tomography (ATP).

3. Results

Fig. 1 indicates that the O content in the ferritic powder increases almost linearly with the increase of O_2 in the Ar atmosphere. At a 0.45 vol.% of O_2 in Ar, there is 0.32 wt.% of O in the powder, while the O content approaches to 1.06 wt.% in the powder at a 1.9 vol.% of O_2 in Ar. Therefore, the O content in the powder is very sensitive to that in the atmosphere. Meanwhile, the O content varies with the particle size. Coarse particles have a much less O content than that in fine particles. In the particles ranging from 74 μm to 147 μm, the average O content is 0.29 wt.%, while in particles smaller than 23 μm, the O content increases to 0.42 wt.%, as shown in Fig. 2. So it seems that small droplets of the steel melt have a faster oxidation rate, perhaps due to their large specific surface area. The X-ray diffraction analyses indicates that there is no detectable oxides in the powder at a O level of 0.3 wt.%, no oxides are found in the powder, even with 1.06 wt.% of O, as shown in Fig. 3. There may be some oxides, like chromium and iron oxides

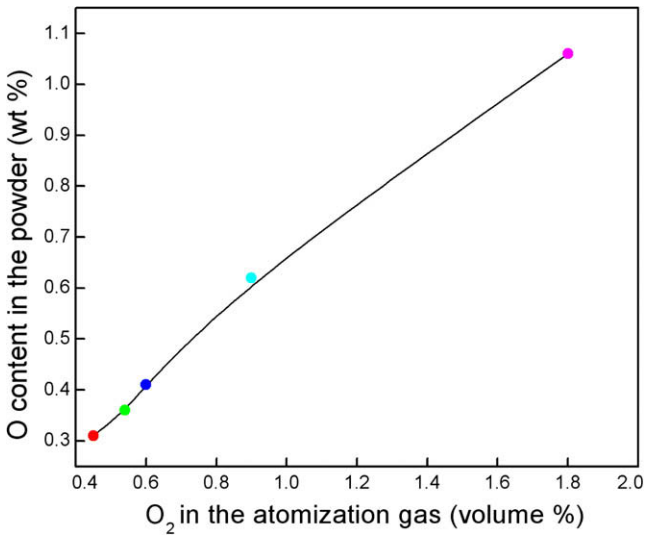

Fig. 1. Oxygen content in powder vs. in atomizing atmosphere.

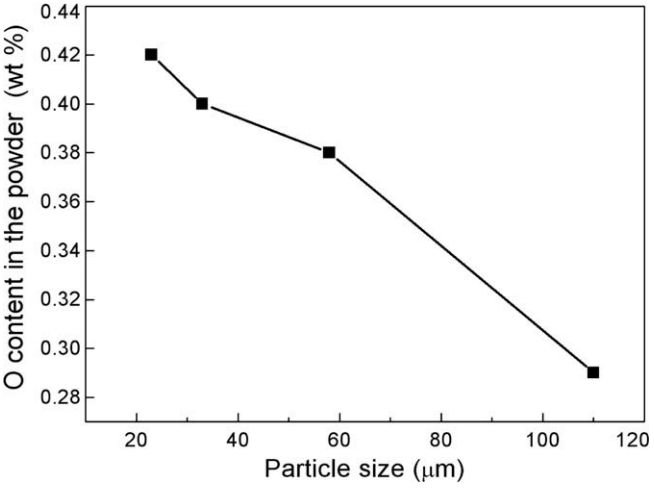

Fig. 2. Oxygen content in powder vs. particle size.

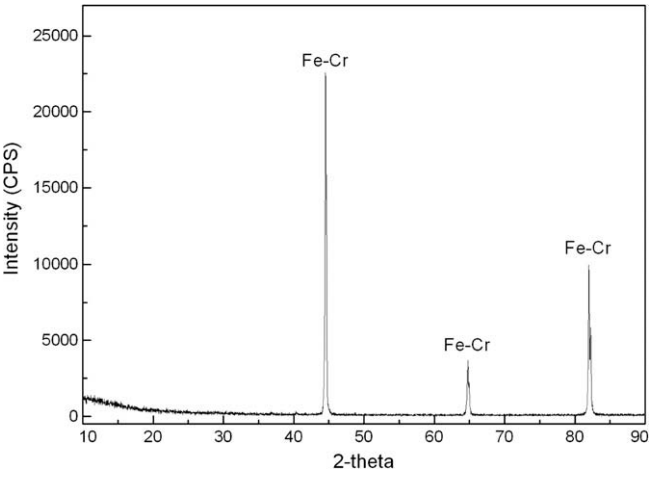

Fig. 3. XRD patterns of powder added with oxygen.

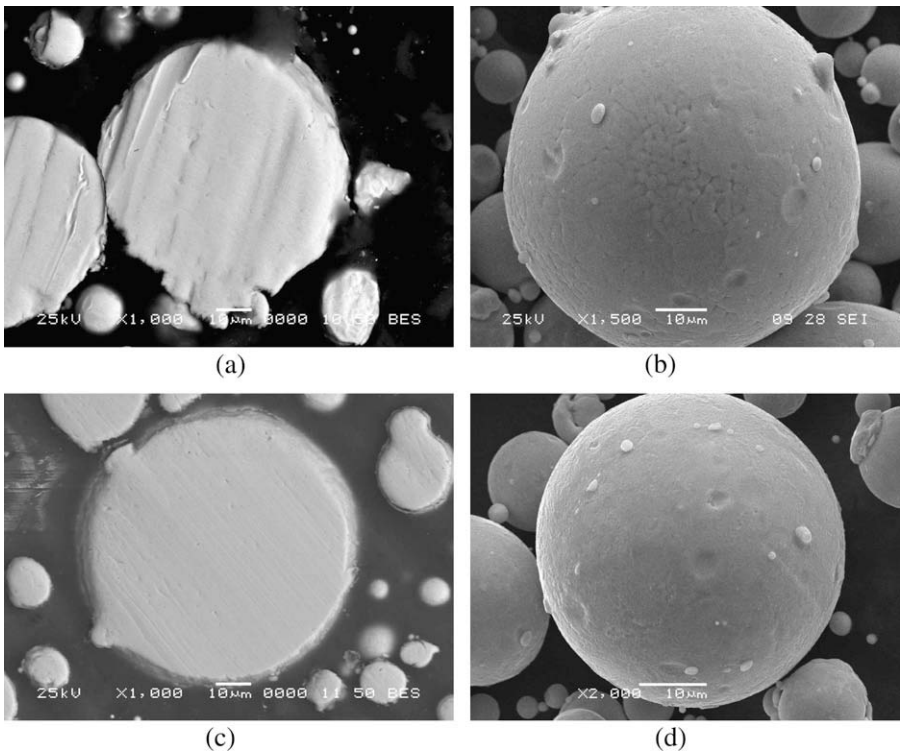

Fig. 4. Microstructures of pre-alloyed powders with different oxygen content: (a) O:300 ppm, microstructure; (b) O:300 ppm, surface morphology; (c) O:3000 ppm, microstructure; (d) O:3000 ppm, surface morphology.

form on the particle surface, but it is difficult to detect due to the small amount and small size. Since nanoclusters were detected in ODS 14YWT containing 0.3 wt.% O, the alloy powder containing the same level of oxygen was selected for further studies. The influence of O content on the microstructure of the particles is indicated in Fig. 4. At a very low level of O content, 0.03 wt.%, the microstructure of the ferritic steel shows a typical solidification feature with dendritic structures. The surface of the particles is very clear, and the dendritic boundaries can be detected, as shown in Fig. 4a and b. As the O content increases to 0.3 wt.%, the microstructure does not change much, however, the surface of the particles is not as clear as that at a low level of O content, and it is hard to see dendritic boundaries. It is believed that particles with a high level of O content are covered with a very thin oxide layer. Fig. 5 shows the O profile of different parts of the particle. There is a gradual change of O content in the particles and the O contents near the surface of the particles are about 0.2 wt.% higher than that inside particles. This may prove that O can be gradually dissolved in the ferritic matrix.

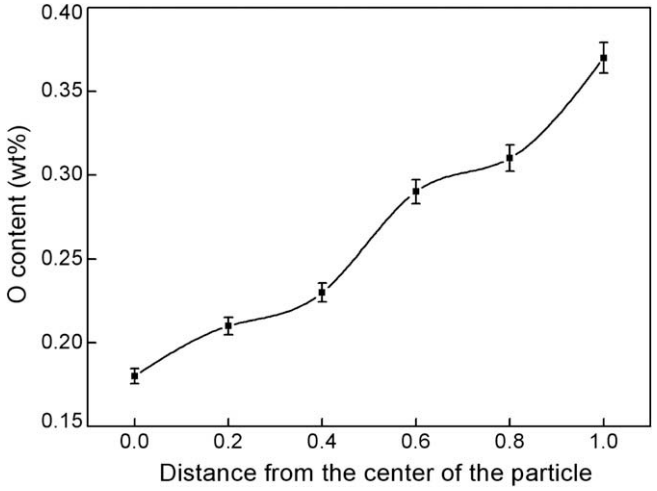

Fig. 5. Oxygen distribution in pre-alloyed particles *r* is the radius of a powder.

After being sintered at 1250 °C for 2 h, the ferritic steel is far from being fully densified. The density is about 85% of the theoretical (7.87 g/cm^3, measured by the ingot), as shown in Table 1. Subsequent hot deformation eliminates the residual porosity significantly. At a reduction of 80%, the relative density approaches to as high as 99% of the theoretical. Further hot-rolling does not change the density. The microhardness of the ferritic steel also indicates the increase of the density. Fig. 6 shows the microstructures of the as-sintered and as-deformed ferritic steel samples. The powders retain their shape in the as-sintered microstructure, and primary particle boundaries can be clearly seen. By a reduction of 30%, the deformation of primary particles occurs; boundaries among small particles begin to be disintegrated. However, large powder particles still maintain their shapes and boundaries. By a reduction of 80%, most primary powder boundaries are disintegrated and large particles are elongated along the flow direction.

Table 1
Density and microhardness of sintered and deformed ferritic steels.

	Sintered	Hot-forged, 30% reduction	Hot-forged, 70% reduction	Hot-rolled, 90% reduction
Density/ (g/cm^3)	6.62	7.41	7.77	7.74
HV	191	204	260	268

Further hot-rolling leads a more homogenous deformation microstructure. Since further hot-rolling does not contribute to an increase of the density, only hot-forged specimens are used for subsequent heat-treatments.

Fig. 7 indicates the microstructures of the ferritic steel after being heat-treated at temperatures ranging from 800 to 1400 °C. The grain boundaries are difficult to be precisely characterized at all temperatures owing to the poor contrast. It can be roughly seen that recrystallization occurs inside the deformed regions at 800 °C, and the primary particle boundaries elongated along the flow direction are rather clear. At 1000 °C, many fine grains recrystallize inside the primary particles. Grain growth occurs at the temperature of 1100 °C, resulting in disappearing and coarsening of the primary powder boundaries due to recrystallization and grain growth occur. At 1200 °C, grains larger than 20 μm can be seen, and at 1400 °C, the microstructure seems to be rather homogenous and no trace of primary particle boundaries can be found. Fig. 8 shows the hardness of the ferritic steel heat-treated at different temperatures. It is interesting to note that the hardness increases fast with the heat-treating temperature, arriving at a peak value of HRC 55 at 1300 °C, almost doubled compared with that at 800 °C. Then, the hardness drops some to HRC 47 at 1400 °C.

More detailed microstructures were observed by TEM. In the as-deformed ferritic steel, it is hard to find precipitates, rather, a high density of dislocations can be observed. For example, Fig. 9a indicates a sub-grain bounded with dislocation walls, and Fig. 9b shows a tangling of highly dense dislocations. In the specimen annealed at 900 °C for 1 h, few large particles (~100 nm) can be found, as shown in Fig. 10a. EDAX shows that it is rich in Ti and O, but it is difficult to determine the exact composition and structure. In specimens annealed at 1300 °C, high density of precipitates can be found, as shown in Fig. 10b. There are two kinds of particle size: 50 nm or larger and 10–20 nm. The large particles are enriched with Ti and O, and the small particles are with Y, Ti and O. After being annealed at 1400 °C, the average size of the particles increases significantly, as shown in Fig. 10c. Most particles are enriched with Y, Ti and O. Some particles, which have faceted shape, are rich in Cr, as shown in Fig. 10d. As many studies have shown the presence of the complex oxides [5,16,17], it can be predicted that the oxides are probably Y-riched, Ti-riched and Cr-riched, respectively. In order to determine if there is any nanoclusters in the ferritic steel, small specimen was cut by using focused ion beam. The O profile examined by Atom Probe Tomography does not shown nanometer-scaled clusters. The figure is not shown here.

4. Discussions

4.1. Formation of precipitates

Though there is limited data on the solubility of oxygen and yttrium in liquid ferritic steel, it can be believed that both of them are dissolved in the melt because liquid metals usually have a high solubility for interstitial elements [18], and yttrium has a solubility up to 1 wt.% in iron at 1500 °C. Other elements, such as Cr, Ti and W can be completely dissolved in the melt judging from the binary phase diagrams [19]. Therefore, in the liquid state, the melt droplet can be considered chemically homogenous. The cooling rate of gas-atomization can be as high as 10^3–10^5 °C/s [20], so the homogenous melt can be frozen by rapid solidification, and the precipitation of oxides and other secondary particles are suppressed. The XRD result of the ferritic powder also indicates a single-phased state in the ferritic steel (Fig. 3). However, the surface of the powder, which was still at high temperatures, may react with the oxygen-containing atomization atmosphere, and form an oxide layer. The oxide layer is too thin to be detected by XRD, but make the microstructure fussy in SEM (Fig. 4). The O profile in the powder also indicates that O is almost homogenously distributed inside

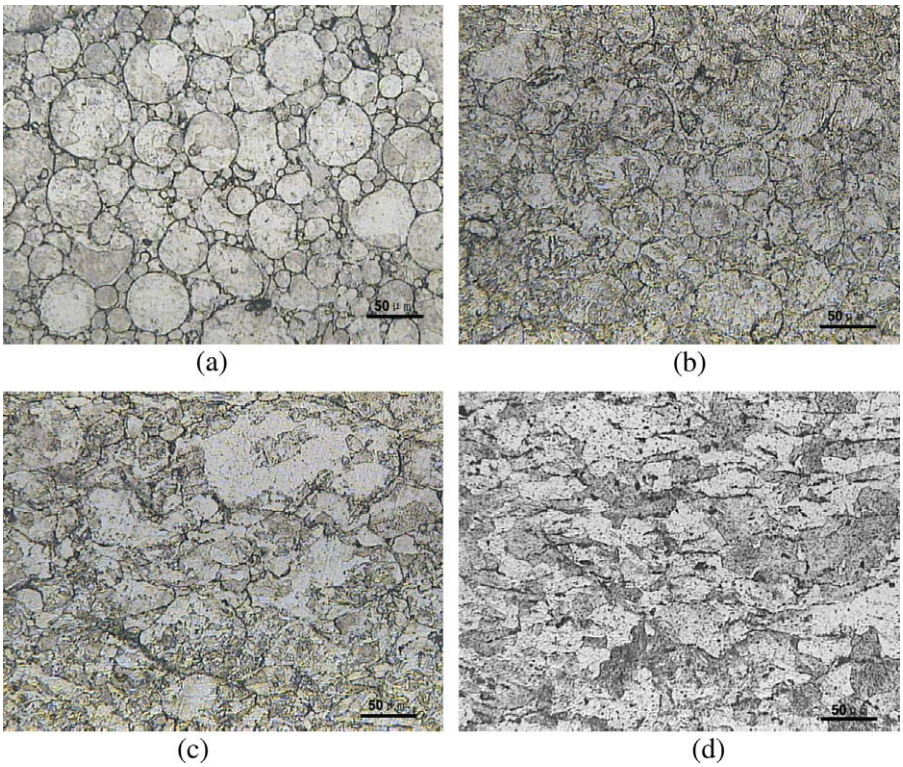

Fig. 6. Microstructures of sintered and deformed ferritic steel: (a) as-sintered; (b) hot-forged, 30% reduction; (c) hot-forged, 70% reduction; (d) hot-rolled, 80% reduction.

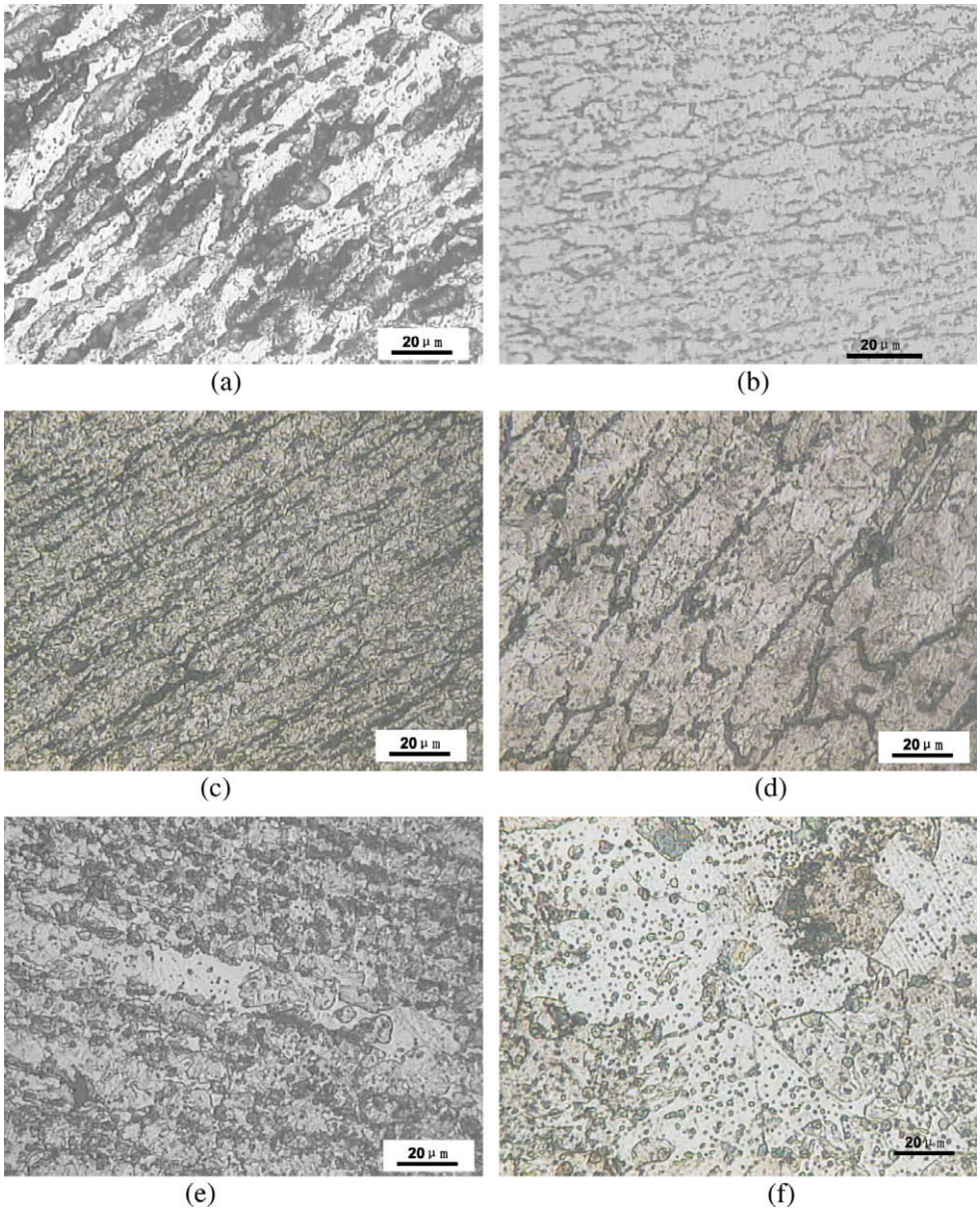

Fig. 7. Microstructures of ferritic steel heat-treated at different temperatures for 1 h: (a) 800 °C; (b) 900 °C; (c) 1000 °C; (d) 1100 °C; (e) 1300 °C; (f) 1400 °C.

the particles, except that the surface has a 0.1 wt.% higher content of O.

The surface oxide layer plays an important role in the microstructural evolution in the ferritic steel. During sintering, the oxide layer may slow down the flow behaviour of particles into the porosity and may hinder the diffusion between the particles, so the density of the sintered compact is rather low and primary particle boundaries do not change at all. Moreover, as O has a very small solubility in solid steel [21], the oxide layer may be stable enough on the surface, and may grow by attracting O inside the particle. This process will prevent the formation of Ti or Y oxides inside the particles even at a sintering temperature of 1250 °C. By thermal deformation, the surface oxide layer can be fragmented depending on the degree of deformation. During the subsequent heat-treatment, high density of dislocations (Fig. 9) promote the non-equilibrium diffusion of alloying elements [22], like in mechanical alloying, thus may lead to a process involving the dissolution of prior oxide layer and nucleation of new oxides. The dissolution and precipitation process of oxides is illustrated in Fig. 11. Since both titanium and yttrium have a high affinity to oxygen, titanium-based oxides and yttrium-based oxides can exist at the same time due to different nucleation sites and local chemical compositions. Perhaps due to a higher affinity to oxygen, Y has a very low solubility in titanium-based oxides; however, titanium can dissolve in yttrium-based oxides, as indicated by the EDAX results. The chemical composition has a significant influence on the growth behaviour of oxides. It has been established that the addition of Ti can refine the yttrium oxides to several nanometers [23,24]. Therefore, there is a bimodal distribution of oxides in the ferritic matrix: large titanium-rich oxide and fine yttrium–titanium-rich oxides. The results also conform to other published work [16]. The size of the oxides also depends on the heat-treatment temperatures. At 900 °C, only large titanium-based oxides can be detected and the yttrium–titanium-based oxides are too small to find. Both of them can be seen as the temperature increases to 1300 °C, while the oxides grow fast at an excessively high temperature of 1400 °C. The precise identification of the oxides in the matrix will be further studied.

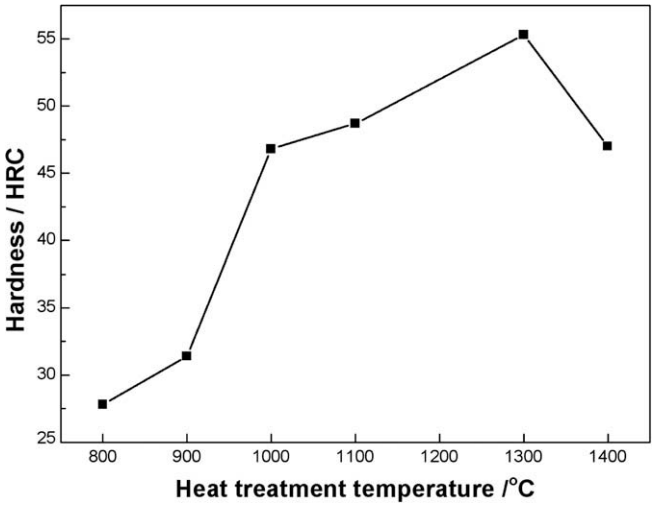

Fig. 8. Microhardness of deformed ferritic steel after heat-treatment at different temperatures.

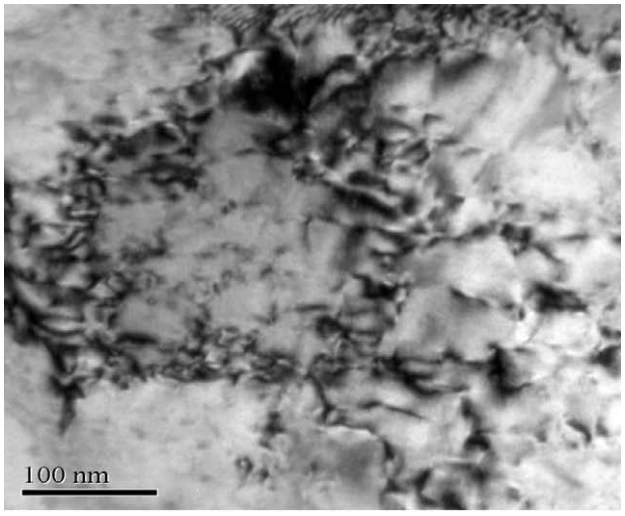

(a)

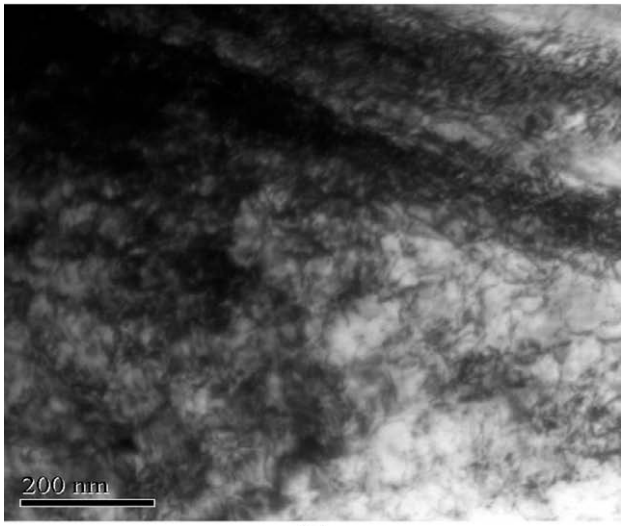

(b)

Fig. 9. TEM microstructures of hot-deformed ferritic steel: (a) sub-grains and (b) high density of dislocations.

In the same 14YWT alloy prepared by mechanical alloying, there are high density of nanoclusters, with a size of 1–2 nm and containing Ti, Y, O and vacancy, dispersed in the ferritic matrix [25]. However, Atom Probe Tomography results show that no such nanocluster was found in the present work. There are two prerequisites for the formation of nanoclusters: atomic-scaled mixing of alloying elements and high density of vacancy. The oxide layer on the particle surface prevent Ti, Y and O from mixing in atomic scale in the ferritic matrix, rather, these elements are in the form of various oxides. Even though the oxide layer is disintegrated by large deformation, the dispersion of alloying elements is far from homogenous like in the process of mechanical alloying. Moreover, the mechanical alloying process provides much more vacancy than the conventional hot deformation [26]. Vacancy is very important for the formation of nanoclusters. The first principle calculation results indicate that by combining with vacancy, Ti–O bonding and Y–Ti–O bonding can be highly stabilized [27]. Also such clusters are very stable, and will not grow at a temperature as high as 1000 °C [28]. In this way, particles as fine as 1–2 nm can exist. Short time of mechanical alloying of the gas-atomized powder would be a useful way for the formation of nanoclusters in the ferritic steel. This work is currently under study and will be published elsewhere.

Moreover, the workability of ODS ferritic steel to fabricate thin wall cladding tube is more important, and it depends on the oxide particles volume fraction, therefore, the improvement or the investigation of the workability and mechanical properties in consolidated form need future work.

4.2. Hardness

For conventional metallic materials, the hardness may decrease with increasing annealing temperatures. However, the ferritic steel in this work does not show any softening until 1400 °C. Two factors may contribute to the hardness of the ferritic steel: recrystallization behaviour and precipitation of oxide particles. It can be seen in Fig. 7 that fine grains form in the deformed microstructure, which will strengthen the matrix. The hardness can be increased with the recrystallization process, which is almost finished at 1000 °C. At 1100 °C, grain growth occurs, which could lead to decrease of the hardness. We recently found that the hardness of the ferritic steel drops with further tempering at a low temperature (for example, 700 °C), so the increase of hardness with heat-treating temperature may be due to the formation of quenching-in vacancy. However, the phenomenon needs further study and will be published elsewhere. As the temperature further increases to 1400 °C, the particles begin to coarsen. Since the hindering effect of particles on the movement of dislocations degrades with the particle size, the strengthening induced by the particles and vacancies cannot compensate for the softening induced by the grain growth any more and the hardness of the ferritic steel begins to drop.

5. Conclusions

This work develops a simple process to prepare oxides dispersion strengthened ferritic steel, and provides some insightful knowledge on the formation of precipitates and their effect on the mechanical behaviour. By studying the microstructural evolution and microhardness of the ferritic steel, the following conclusions can be drawn:

(1) By adjusting the volume content of O_2 in the gas atmosphere Ar, the O level in the ferritic powder can be well controlled. The O dissolves uniformly in the ferritic powder, and a very thin layer of oxides forms on the powder surface.

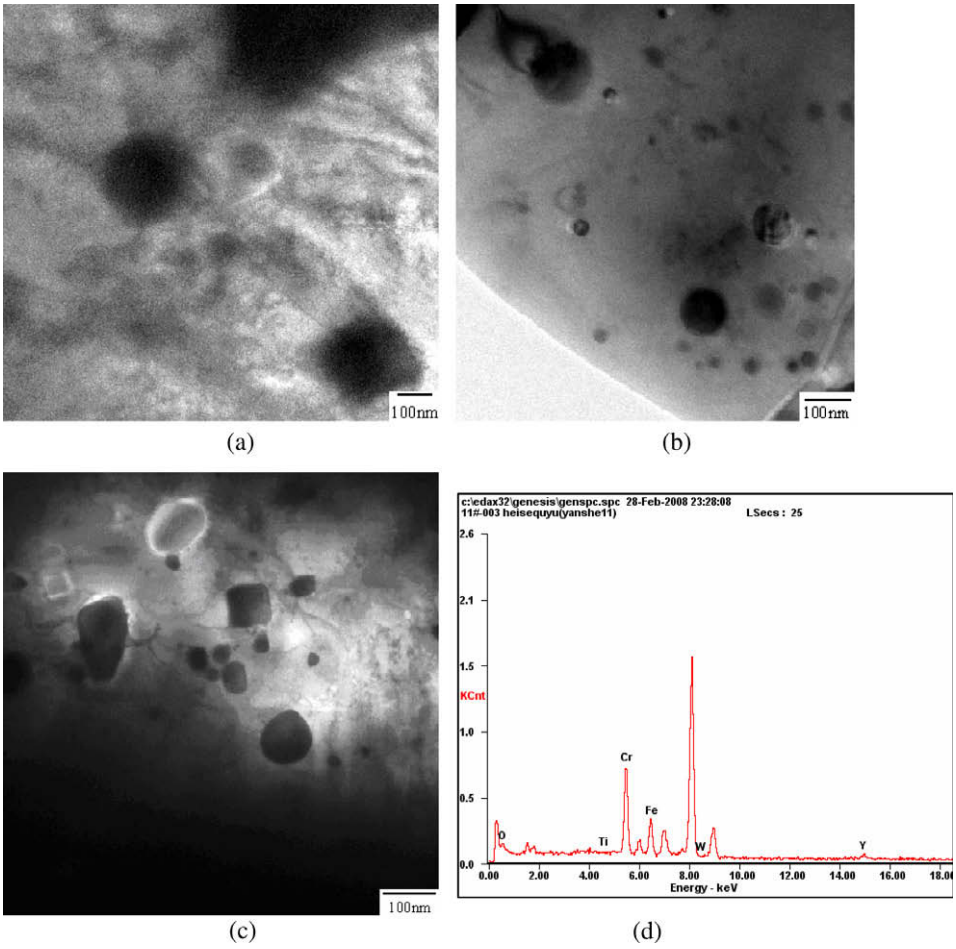

Fig. 10. TEM microstructures of heat-treated ferritic steel: (a) 900 °C; (b) 1300 °C; (c) 1400 °C; (d) EDAX detection of particles with faceted shape in (c).

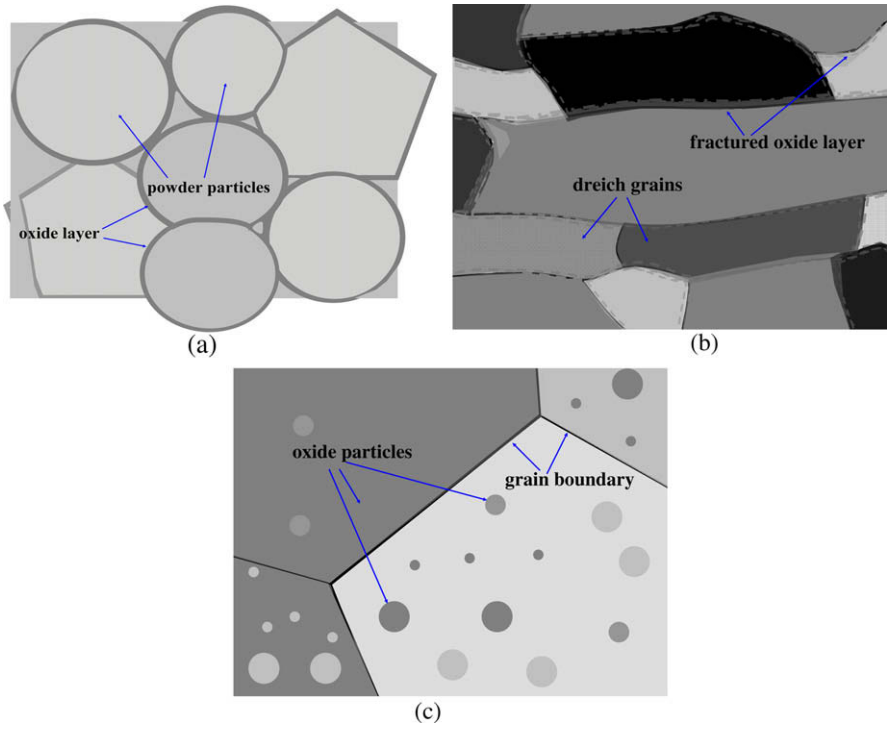

Fig. 11. Illustration on the formation of precipitates in ferritic steel: (a) stable oxide layer on primary particles; (b) fragmentation of oxide layer by thermal deformation; (c) formation of oxides.

(2) It is difficult to eliminate the primary particle boundaries and obtain a high density by conventional sintering. After hot deformation in a large reduction, the primary particle boundaries can be disintegrated and a relative density as high as 99% of the theoretical can be obtained.
(3) The oxide layer on the powder surface has a significant effect on the microstructural evolution. It may prevent the diffusion in between the primary particles during sintering. After being disintegrated and homogenously dispersed in the ferritic matrix, it may dissolve and/or induce the nucleation of new oxides. Depending on different nucleation site and local chemical compositions, two kinds of oxide particles form in the ferritic steel: large (~100 nm) Ti-rich and fine (10–20 nm) Y–Ti-rich oxides.
(4) The hardness of the ferritic steel increases with increasing annealing temperatures. There are two factors influencing the hardness: recrystallization behaviour and precipitation of oxide particles. At an excessively high temperature, the coarsening of precipitates occurs, and the strengthening effect induced by the precipitates cannot compensate for the softening induced by the grain growth, the hardness of the ferritic steel degrades.

Acknowledgements

This work is supported by the Natural Science Foundation of China under Contract Nos: 50634060 and 50721003. The authors are grateful to Prof. M.K. Miller from Oak Ridge National Laboratory for his help on TAP and Prof. Huiren Jiang in Beijing University of Aeronautic and Astronautic for his help on TEM. One of the authors Yong Liu also thanks for the support of Alexander von Humboldt Fellowship.

References

[1] C.P.C. Wong, S. Malang, M. Sawan, I. Sviatoslavsky, E. Mogahed, S. Smolentsev, S. Majumdar, B. Merrill, R. Mattas, M. Friend, J. Bolin, S. Sharafat, Fusion Eng. Des. 72 (2004) 245–275.
[2] Steven J. Zinkle, Fusion Eng. Des. 74 (2005) 31–40.
[3] S. Mohamed, El-Genk, Jean-Michel Tournier, J. Nucl. Mater. 340 (2005) 93–112.
[4] I.G. Wright, T.B. Gibbons, Int. J. Hydrogen Energy 32 (2007) 3610–3621.
[5] G.R. Odette, M.J. Alinger, B.D. Wirth, Rev. Mater. Res. 38 (2008) 471–503.
[6] R.L. Klueh, J.P. Shingledecker, R.W. Swindeman, D.T. Hoelzer, J. Nucl. Mater. 341 (2005) 103–114.
[7] S. Ukai, T. Nishida, T. Okuda, T. Yoshitake, J. Nucl. Mater. 258–263 (1998) 1745–1749.
[8] S. Ukai, M. Harada, H. Okada, M. Inoue, S. Nomura, S. Shikakura, K. Asabe, T. Nishida, M. Fujiwara, J. Nucl. Mater. 204 (1993) 65–73.
[9] M.K. Miller, D.T. Hoelzer, E.A. Kenik, K.F. Russell, Intermetallics 13 (2005) 387–392.
[10] A. Wasilkowska, M. Bartsch, U. Messerschmidt, R. Herzog, A. Czyrska-Filemonowicz, J. Mater. Process. Technol. 133 (2003) 218–224.
[11] G. Yu, N. Nita, N. Baluc, Fusion Eng. Des. 75–79 (2005) 1037–1041.
[12] R. Lindau, A. Möslang, M. Rieth, M. Klimiankou, E. Materna-Morris, A. Alamo, A.-A.F. Tavassoli, C. Cayron, A.-M. Lancha, P. Fernandez, N. Baluc, R. Schäublin, E. Diegele, G. Filacchioni, J.W. Rensman, B.v.d. Schaaf, E. Luconind, W. Dietz, Fusion Eng. Des. 75–79 (2005) 989–996.
[13] B.N. Goshchitskii, V.V. Sagaradze, V.I. Shalaev, V.L. Arbuzov, Yun Tian, Wan Qun, J. Nucl. Mater. 307–311 (2002) 783–787.
[14] H. Sakasegawa, S. Ohtsuka, S. Ukai, H. Tanigawa, M. Fujiwara, H. Ogiwara, A. Kohyamad, Fusion Eng. Des. 81 (2006) 1013–1018.
[15] M.J. Alinger, G.R. Odette, D.T. Hoelzer, Acta Mater. 57 (2009) 392–406.
[16] P. Miao, G.R. Odette, T. Yamamoto, M. Alinger, D. Hoelzer, D. Gragg, J. Nucl. Mater. 367–370 (2007) 208–212.
[17] M. Klimiankou, R. Lindau, A. Möslang, J. Nucl. Mater. 329–333 (2004) 347–351.
[18] M.K. Miller, D.T. Hoelzer, E.A. Kenik, K.F. Russell, J. Nucl. Mater. 329–333 (2004) 338–341.
[19] T.B. Massalski, J.L. Murry, L.H. Bennett, Hugh Baker Binary Alloy Phase Diagram, ASM International, OH, Metals Park, 1987, p. 822, 1118, 1124, 1126.
[20] N. Zeoli, S. Gu, Comput. Mater. Sci. 42 (2008) 245–258.
[21] S. Ohtsuka, S. Ukai, M. Fujiwara, T. Kaito, T. Narita, J. Phys. Chem. Solids 66 (2005) 571–575.
[22] C. Cayron, E. Rath, I. Chu, S. Launois, J. Nucl. Mater. 335v (2004) 83–102.
[23] J.H. Schneibel, S. Shim, Mater. Sci. Eng. A 488 (2008) 134–138.
[24] J.H. Schneibel, C.T. Liu, D.T. Hoelzer, M.J. Mills, P. Sarosi, T. Hayashi, U. Wendt, H. Heyse, Scr. Mater. 57 (2007) 1040–1043.
[25] T.R. Allena, J. Gan, J.I. Cole, M.K. Miller, J.T. Busby, S. Shutthanandan, S. Thevuthasan, J. Nucl. Mater. 375 (2008) 26–37.
[26] Y. Ortega, V. de Castro, M.A. Monge, A. Muñoz, T. Leguey, R. Pareja, J. Nucl. Mater. 376 (2008) 222–228.
[27] C.L. Fu, Maja Krcmar, G.S. Painter, Phys. Rev. Lett. 99 (2007) 225502/1-4.
[28] M.K. Miller, K.F. Russell, D.T. Hoelzer, J. Nucl. Mater. 351 (2006) 261–268.